Energy Loss of α Particles in Noble Gases from 0.3 to 2.0 MeV*

W. K. Chu and D. Powers
Baylor University, Waco, Texas 76703
(Received 23 October 1970)

Stopping cross sections of gaseous He, Ne, Ar, Kr, and Xe for α particles of 300 keV to 2 MeV have been measured in a differentially pumped gas cell and checked in a sealed gas cell. The results agree with Weyl's measurements in He from 1 to 5%, with Weyl's measurements in Ar from 4.7 to 6.9%, and with Bichsel's measurements in Ar from -2.8 to $+5.5$%. The measurements agree over the entire energy region for all gases except He to better than 16% with the Lindhard-Winther theory modified by a Hartree-Fock-Slater electron charge distribution, and to better than 24% with Bonderup's theory with the same modification.

I. INTRODUCTION

Since 1963 several experiments[1] have shown that the electronic stopping cross section ϵ_{ion} has an oscillating dependence on the atomic number of the ion. An experiment[2] performed in this laboratory indicated a structure in the dependence of the α-particle stopping cross section ϵ_α on the atomic number of target Z_2 in the region $Z_2 = 22-29$.

The present paper reports part of a series of experiments proposed to measure the α-particle stopping cross section in elements in order to obtain more information about the dependence of ϵ_α on Z_2 and energy, and in particular, to see if additional anomalous structure exists.

II. EXPERIMENTAL PROCEDURE AND ACCURACY OF MEASUREMENTS

The detailed experimental method and arrangement for the stopping-cross-section measurements in gases are given in a previous paper.[3] In brief, an α-particle beam obtained from a 2-MeV Van de Graaff accelerator is focused by a quadrupole magnet and analyzed by a 10° magnet and then is passed through a differentially pumped gas-cell system into a 20° analyzing magnet for energy determination. The pressure of the gas cell, which is varied from 0.8 to 9.3 mm Hg, is measured with a McLeod gauge, and the temperature, with a mercury-in-glass thermometer. The research-grade gases were supplied by Matheson, Co., La Porte, Texas, and were of purity greater than 99.995%

End corrections of 0.6 to 1.98% for ϵ_{He}, 0 to 1.74% for ϵ_{Ne}, and 0 to 1.3% for ϵ_{Ar} were made for the gas cell in the differential pumping system as in the previous experiment; no corrections were needed for the Kr and Xe measurements. The effects of multiple scattering and localized heating of the gas were shown to be small ($\lesssim 0.1$%) in the previous experiment. The α-particle distributions with gas in the cell were symmetric as before, and the most probable energy loss was used in calculating stopping cross sections. These cross sections were obtained at an energy E_α intermediate between the initial energy E_i and final energy E_f which differed by at most 0.6% from the average energy $E_{av} = \frac{1}{2}(E_i + E_f)$. This small difference was taken into account in all the measurements.

A McLeod gauge (Model GM-100A, Bendix Vacuum Corp., Rochester, N.Y.) containing triply distilled mercury was used and was replaced periodically by a second identical gauge to ensure cleanliness of the internal glassware while the first gauge was being cleaned by a professional glassblower, and to eliminate the introduction of systematic errors through inhomogeneities in the capillaries or through the absolute pressure calibration of the gauge. Pressures ranged from 2.8 to 9.3 mm Hg in the He, Ne, and Ar measurements and from 0.84 to 2.4 mm Hg in the Kr and Xe measurements. Readings on the two gauges, compared throughout the course of the experiment over the above pressure range, disagreed to less than 0.9% for the Kr and Xe pressure region and less than 0.5% for the He, Ne, and Ar pressure region. When the two gauges were used simultaneously in a pressure measurement, the average of the two readings was always used.

Independent energy-loss measurements for Ar, Kr, and Xe were also made in a sealed gas cell in an 18-in. scattering chamber using a solid-state detector and multichannel pulse-height analyzer, as in the previous experiment,[3] to test the reliability of the differentially pumped gas-cell measurements and to ensure that no systematic errors were being introduced due to slit effects, heating effects, 20°-magnet energy dispersion, gas-cell length, etc. In principle, all systematic errors except those in the incident-energy scale and in the McLeod gauges and thermometers themselves should be eliminated in these separate measurements. The solid-state detector measurements (probable error ± 3.6 to ± 4.5%) were not as accurate as the differentially pumped gas-cell measurements (probable error in the individual measurements was

± 1.5 to $\pm 2.3\%$ as shown in the previous experiment), but did agree with one another within this specified accuracy and thus enhanced the reliability of the present measurements.

III. RESULTS

The number of data points N obtained for each gas varied from 190 (Xe) to 411 (Ar) and is given as the last entry in Table I. When several measurements of ϵ were obtained at the same intermediate energy E_α, the average value ϵ_{av} of these measurements was found, and the 1.5 to 2.3% probable error for a single measurement was reduced by $\sqrt{n}$, where n is the number of ϵ measurements at E_α. The number n, typically 2 or 3, was as high as 13. A least-squares fit to a fifth-degree polynomial[4] was made by minimizing the sum

$$\sum_{k=1}^{K} w_k[(\epsilon_{av})_k - a_0 - a_1 E_k - a_2 E_k^2 - a_3 E_k^3 - a_4 E_k^4 - a_5 E_k^5]^2 ,$$

where $(\epsilon_{av})_k$ is the average measured stopping cross section at energy E_k, and where the weighting factor w_k is inversely proportional to the variance of a single measurement; that is to say, w_k is proportional to n. If only one measurement existed at E_k, then $(\epsilon_{av})_k = \epsilon_k$, the experimental measurement at that point, and $w_k \propto 1$. K represents the number of data points after the averaging process to determine the curve, and was of the order of 80 to 90. The curve-fit parameters are tabulated in Table I for the energy region $0.3 \le E \le 2.0$ MeV, except for Ne and Kr, where the lower limit is 0.35 MeV. The reason for the 0.35 MeV for Ne and Kr is that the curve for these two gases did not follow the experimental trend of points below 0.35 MeV, but did for all other energies. Attempts were made at fitting the data to polynomials of all degrees from two to eight, but the fifth-degree polynomial was best except for Ne, where a fourth-degree polynomial gave the best fit. The standard deviation σ for each curve in 10^{-15} eV cm^2 is also given in Table II and was calculated from

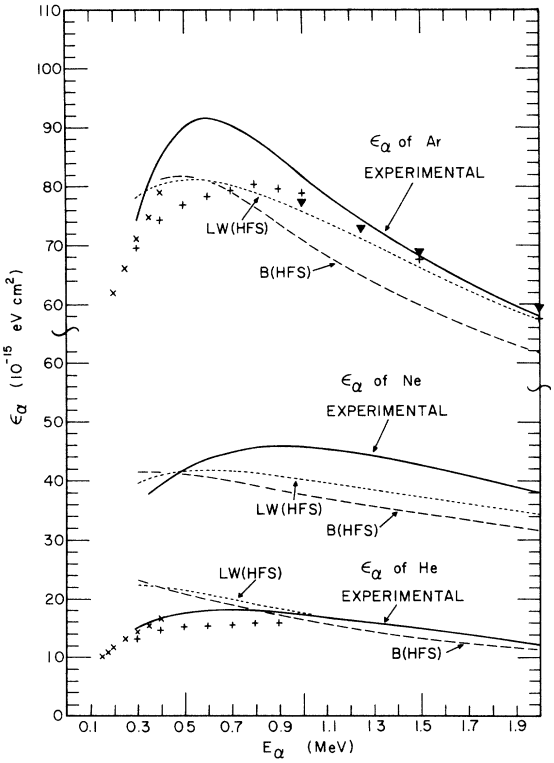

FIG. 1. Stopping cross sections ϵ_α as a function of energy E_α for He, Ne, and Ar. The heavy solid curves are the present experimental measurements as fitted to a fourth- or fifth-degree polynomial. The x's are measurements by Weyl (Ref. 5), the +'s by Weyl and Burgy (Ref. 7), and ▼'s by Bichsel *et al.* (Ref. 6). The curves B(HFS) and LW(HFS) are the theories of Bonderup and of Lindhard and Winther, respectively, based on a charge density calculated from Hartree-Fock-Slater wave functions.

$$\left(\sum_{k=1}^{K} w_k[(\epsilon_{av})_k - \epsilon_k^{curve}]^2\right) \Big/ \left(\sum_{k=1}^{K} w_k\right) ,$$

where ϵ_k^{curve} is the value of the curve at energy E_k. The probable error in ϵ^{curve} is given as $0.6745 \times [\sigma/\bar{\epsilon}_{expt}] \times 100\%$, where

TABLE I. Curve-fit parameters for $\epsilon = a_0 + a_1E + a_2E^2 + a_3E^3 + a_4E^4 + a_5E^5$, where ϵ is in 10^{-15} eV cm^2, E is in MeV, $0.3 \le E \le 2.0$ MeV, except for Ne and Kr, where $0.35 \le E \le 2.0$ MeV. σ is the standard deviation of the curve in 10^{-15} eV cm^2. N is the total number of data points for a given gas.

Gas	a_0	a_1	a_2	a_3	a_4	a_5	σ	Probable error in ϵ[a] (%)	N
He	3.4209	64.124	−102.97	77.502	−29.028	4.2864	0.23	0.96	270
Ne	20.684	68.064	−61.94	21.959	−2.9066	0.0000	0.44	0.70	228
Ar	−9.2286	463.98	−770.52	574.88	−206.04	28.718	0.61	0.53	411
Kr	−16.889	586.44	−985.68	763.82	−287.26	42.288	1.43	0.99	265
Xe	42.827	513.63	−863.50	650.68	−235.84	33.274	1.65	0.82	190

[a]Probable error in ϵ is $0.6745(\sigma/\bar{\epsilon}_{expt}) \times 100\%$, where $\bar{\epsilon}_{expt} = \left(\sum_{k=1}^{K} w_k (\epsilon_{av}^{expt})_k\right) \Big/ \sum_{k=1}^{K} w_k$.

TABLE II. Experimental and theoretical values of the stopping cross section. Column 1 gives the stopping material, column 2 the α-particle energy, column 3 the curve-fitted experimental stopping cross section ϵ_{expt} in 10^{-15} eV cm^2, column 4 the stopping cross section calculated by using the Lindhard-Winther theory with the Hartree-Fock-Slater charge distribution for the stopping atom, and column 5 the percentage difference between the LW(HFS) theory and the experimental result. Column 6 gives the stopping cross section calculated by using Bonderup's theory with the Hartree-Fock-Slater charge distribution for the stopping atom, and column 7 the percentage difference between the B(HFS) theory and the experimental result.

Gas	Energy (MeV)	ϵ_{expt} (10^{-15} eV cm^2)	$\epsilon_{LW(HFS)}$ (10^{-15} eV cm^2)	$100(\epsilon_{expt}-\epsilon_{LW})/\epsilon_{expt}$ (%)	$\epsilon_{B(HFS)}$ (10^{-15} eV cm^2)	$100(\epsilon_{expt}-\epsilon_{B})/\epsilon_{expt}$ (%)
He	0.3	15.3	22.5	−47.5	23.3	−52.7
	0.4	16.9	22.1	−31.1	22.1	−31.1
	0.5	17.7	21.6	−21.7	21.0	−18.3
	0.6	18.1	20.9	−15.2	20.0	−10.3
	0.7	18.2	20.1	−10.5	19.0	−4.5
	0.8	18.0	19.3	−7.1	18.1	−0.5
	0.9	17.7	18.5	−4.5	17.2	2.9
	1.0	17.3	17.8	−2.7	16.5	4.8
	1.1	16.9	17.1	−1.1	15.8	6.6
	1.2	16.5	16.4	0.5	15.1	8.4
	1.3	16.0	15.8	1.5	14.5	9.6
	1.4	15.6	15.3	1.8	13.9	10.8
	1.5	15.1	14.7	2.6	13.4	11.2
	1.6	14.6	14.2	2.6	12.9	11.5
	1.7	14.0	13.7	2.4	12.5	10.9
	1.8	13.5	13.3	1.4	12.1	10.3
	1.9	13.0	12.9	0.5	11.7	9.7
	2.0	12.5	12.5	•••	11.3	9.8
Ne	0.35	37.8	40.4	−6.9	41.4	−9.5
	0.4	39.3	41.1	−4.5	41.5	−5.5
	0.5	41.8	41.8	•••	41.3	1.2
	0.6	43.6	41.8	4.1	40.9	6.2
	0.7	44.8	41.7	6.9	40.0	10.7
	0.8	45.5	41.2	9.5	39.3	13.7
	0.9	45.9	40.7	11.3	38.5	16.1
	1.0	45.9	40.2	12.3	37.7	17.8
	1.1	45.6	39.6	13.1	36.9	19.0
	1.2	45.1	39.1	13.3	36.2	19.7
	1.3	44.4	38.4	13.6	35.6	19.9
	1.4	43.7	37.8	13.4	35.1	19.6
	1.5	42.8	37.2	13.1	34.5	19.4
	1.6	41.9	36.6	12.7	34.0	18.9
	1.7	41.0	36.0	12.2	33.4	18.5
	1.8	40.1	35.4	11.6	32.8	18.1
	1.9	39.1	34.8	11.1	32.2	17.7
	2.0	38.2	34.3	10.3	31.6	17.3
Ar	0.3	74.5	78.1	−4.8	81.9	−9.9
	0.4	84.9	80.4	5.3	81.0	4.6
	0.5	90.0	81.3	9.7	81.5	9.5
	0.6	91.5	81.1	11.3	81.1	11.3
	0.7	90.5	80.2	11.4	78.9	12.9
	0.8	88.2	79.0	10.4	76.7	13.0
	0.9	85.1	77.5	8.9	73.8	13.3
	1.0	81.8	75.8	7.3	70.9	13.3
	1.1	78.6	74.0	5.8	68.3	13.1
	1.2	75.6	72.2	4.5	66.1	12.6
	1.3	72.9	70.2	3.7	63.7	12.7
	1.4	70.5	68.3	3.2	61.7	12.5
	1.5	68.3	66.2	3.1	59.5	12.9
	1.6	66.1	64.2	2.9	57.7	12.8
	1.7	64.0	62.3	2.7	56.1	12.4

TABLE II (*Continued*).

Gas	Energy (MeV)	ϵ_{expt} (10^{-15}eV cm^2)	$\epsilon_{LW(HFS)}$ (10^{-15}eV cm^2)	$100(\epsilon_{expt}-\epsilon_{LW})/\epsilon_{expt}$ (%)	$\epsilon_{B(HFS)}$ (10^{-15}eV cm^2)	$100(\epsilon_{expt}-\epsilon_{B})/\epsilon_{expt}$ (%)
Ar	1.8	61.9	60.5	2.2	54.4	12.1
	1.9	59.8	58.9	1.5	52.9	11.6
	2.0	58.0	57.3	1.3	51.7	10.9
Kr	0.35	96.3	99.6	3.4	103.6	−7.6
	0.4	101.9	100.7	1.2	103.1	−1.1
	0.5	108.8	101.6	6.6	102.8	5.5
	0.6	111.2	101.2	9.0	100.0	10.1
	0.7	110.8	100.2	9.5	96.8	12.6
	0.8	108.7	98.2	9.7	93.3	14.2
	0.9	105.8	96.2	9.1	89.5	15.4
	1.0	102.7	93.9	8.6	86.4	15.9
	1.1	99.7	91.4	8.3	84.0	15.7
	1.2	96.9	88.9	8.3	80.9	16.5
	1.3	94.4	86.4	8.4	78.6	16.7
	1.4	92.0	84.1	8.6	76.4	17.0
	1.5	89.8	81.8	8.9	74.5	17.0
	1.6	87.5	79.7	8.9	72.6	17.0
	1.7	85.3	77.7	8.9	70.7	17.1
	1.8	83.2	75.9	8.8	68.9	17.2
	1.9	81.6	74.2	9.0	67.4	17.4
	2.0	80.9	72.5	10.4	65.9	18.5
Xe	0.3	134.9	127.1	5.8	136.5	−1.2
	0.4	146.1	131.9	9.7	135.8	7.0
	0.5	151.4	133.2	12.0	133.2	12.0
	0.6	152.7	132.5	13.2	128.2	16.1
	0.7	151.4	130.3	13.9	123.7	18.3
	0.8	148.5	127.4	14.2	119.0	19.9
	0.9	144.9	124.3	14.2	115.1	20.6
	1.0	141.1	120.8	14.4	111.5	21.0
	1.1	137.3	117.5	14.4	107.6	21.7
	1.2	133.9	114.2	14.7	104.6	21.9
	1.3	130.7	111.2	14.9	101.8	22.1
	1.4	127.9	108.5	15.1	99.3	22.3
	1.5	125.2	105.8	15.5	97.2	22.3
	1.6	122.6	103.5	15.6	94.8	22.7
	1.7	120.0	101.2	15.6	92.5	22.9
	1.8	117.4	99.2	15.5	90.3	23.1
	1.9	114.9	97.3	15.3	88.3	23.2
	2.0	112.9	95.4	15.5	85.9	23.9

$$\bar{\epsilon}_{expt}=\left(\sum_{k=1}^{K} w_k(\epsilon_{av})_k\right)\Big/\left(\sum_{k=1}^{K} w_k\right) \quad .$$

Stopping cross sections for each gas as obtained from the curve fit are tabulated at 100-keV intervals in Table II and are plotted in Figs. 1 and 2 as the heavy solid curves. In Fig. 1 the measurements by Weyl[5] of α particles in Ar and He are plotted as ×'s and the measurements of α particles in Ar by Bichsel *et al.*[6] are plotted as ▾'s. The stopping cross sections of He and Ar for α particles measured by Weyl and Burgy as quoted by Porat and Ramavataram[7] are plotted as +'s. The values are tabulated in Table III for comparison, and the present measurements are seen to be from 0.6% to 14.9% higher than those by Weyl and Burgy, and by 1.2% to 6.9% higher than those of Weyl. The measurements in Ar by Bichsel *et al.*, with accuracy of 1.5% at 1.25 MeV to 0.3% at 2 MeV, disagree with the present measurements at 2 MeV by − 2.8%, by − 0.6% at 1.5 MeV, and by + 5.5% at 1 MeV.

Measurements of proton stopping cross sections in noble gases below 500 keV can be converted to α-particle stopping cross sections corresponding to α particles of the same velocity and by using the ratio $\epsilon_\alpha/\epsilon_p$ suggested by Whaling[8] or more recently given by Bourland and Powers[9] for $E_\alpha = 2.0$ to 0.4 MeV which joins rather smoothly the ratio $\epsilon_\alpha/\epsilon_p$ by Sautter and Zimmerman[10] and by Park and Zimmerman.[11] There exist triton stopping power measurements[12] in Ar, Kr, and Xe which agree

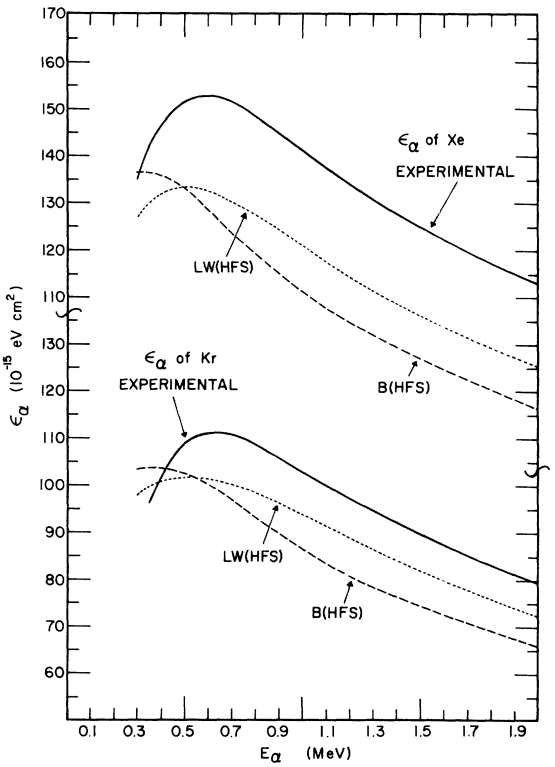

FIG. 2. Same as Fig. 1 except for Kr and Xe.

within experimental accuracy to the proton stopping power measurements at the same velocity by Reynolds *et al.*[13] below 500 keV. Recent proton measurements in Ar, Kr, and Xe by Swint *et al.*[14] are 600 keV or higher in energy (corresponding to α-particle energy greater than 2400 keV) and are outside the region of the present measurements. Their measurements, however, generally join smoothly the measurements by Reynolds *et al.*, and we have therefore compared these latter measurements at a velocity equivalent to the α-particle velocity to the present measurements over the entire energy region $E_\alpha = 0.4$ to 2.0 MeV. The average value of the ratio $\epsilon_\alpha/\epsilon_p$ agrees with the curve given by Bourland and Powers to within 2.6% although at $E_\alpha = 0.4$ MeV, $\epsilon_\alpha/\epsilon_p$ for He is 9% lower and for Xe is 12% higher than their curve.

Rousseau, Chu, and Powers[15] have recently calculated the stopping cross section of α particles in target materials of atomic number $2 \leq Z_{\text{targ}} \leq 54$ by using the theories of Bonderup[16] and of Lindhard and Winther,[17] except by using a spherically averaged electronic charge density obtained from Hartree-Fock-Slater wave functions.[18] These theoretical predictions are plotted as a dotted curve [labeled LW (HFS)] for Lindhard-Winther using Hartree-Fock-Slater wave functions and as a dashed curve [labeled B(HFS)] for Bonderup using the same wave functions. The interesting result is that the Lindhard-Winther prediction gives the qualitative shape of the experimental curves, with the maximum ϵ occurring in the same vicinity as the experimental ϵ does. The Bonderup theory with the Hartree-Fock-Slater modification agrees with the experiment for all gases except He over the entire energy region to better than 24% and the Lindhard-Winther theory with HFS modification to better than 16%. We have tabulated the theoretical values with HFS modification in Table II.

TABLE III. Comparison of present measurements of α-particle stopping cross sections in Ar and He to those by Weyl (Ref. 5), Weyl and Burgy (Ref. 7), and Bischsel *et al.* (Ref. 6). Entries A, B, C, and D are given in 10^{-15} eV cm^2.

Gas	Energy (keV)	A Present measurements	B Weyl and Burgy	$100(A-B)/A$ (%)	C Weyl	$100(A-C)/A$ (%)	D Bichsel *et al.*	$100(A-D)/A$ (%)
He	300	15.3	13.2	13.7	14.5	5.2	...	...
	400	16.9	14.7	13.0	16.7	1.2	...	...
	500	17.7	15.3	13.6	...	...	...	...
	600	18.1	15.4	14.9	...	...	...	...
	700	18.2	15.7	13.7	...	...	...	...
	800	18.0	16.0	11.1	...	...	...	...
	900	17.7	16.0	9.6	...	...	...	...
Ar	300	74.5	69.6	6.3	71.0	4.7	...	...
	400	84.9	74.5	12.2	79.0	6.9	...	...
	500	90.0	77.0	14.4	...	...	...	...
	600	91.5	78.4	14.3	...	...	...	...
	700	90.5	79.5	12.2	...	...	...	...
	800	88.2	80.3	8.9	...	...	...	...
	900	85.1	79.5	6.6	...	...	...	...
	1000	81.8	79.0	3.4	...	...	77.3	5.5
	1250	74.2	73.6	0.8	...	...	72.9	1.8
	1500	68.3	67.9	0.6	...	...	68.7	−0.6
	2000	58.0	57.5	0.9	...	...	59.6	−2.8

*Research supported in part by the National Science Foundation.

[1]Several papers have been published on the observation of the oscillating dependence of ϵ_{ion} on the atomic number. Descriptions and references are given in an earlier paper (see Ref. 2).

[2]W. K. Chu and D. Powers, Phys. Rev. 187, 478 (1969).

[3]P. D. Bourland, W. K. Chu, and D. Powers, Phys. Rev. B 3, 3625 (1971).

[4]The use of a polynomial curve fit was kindly suggested by L. Wine (private communication), Hollins College, Hollins College, Va., and author of the text *Statistics for Scientists and Engineers* (Prentice-Hall, Englewood Cliffs, N. J., 1964). It is, of course, desirable to use a curve based on some physical theory, but there exists no simple analytic function which represents ϵ over the entire energy interval 300 keV to 2 MeV. The polynomial curve fit at least allows a statistical analysis of the experimental data to be made; the curve-fit parameters should not be used outside the experimental energy region.

[5]P. K. Weyl, Phys. Rev. 91, 289 (1953).

[6]H. Bichsel, C. C. Hanke, and J. Buechner, Report No. USC-136-148, 1969 (unpublished).

[7]D. I. Porat and K. Ramavataram, Proc. Phys. Soc. (London) A252, 394 (1960).

[8]W. Whaling, in *Handbüch der Physik*, edited by S. Flügge (Springer-Verlag, Berlin, 1958), Vol. 34, p. 193.

[9]P. D. Bourland and D. Powers, Phys. Rev. B 3, 3635 (1971).

[10]C. A. Sautter and E. J. Zimmerman, Phys. Rev. 140, A490 (1965).

[11]John T. Park and E. J. Zimmerman, Phys. Rev. 131, 1611 (1963).

[12]R. L. Wolke, W. N. Bishop, E. Eichler, N. R. Johnson, and G. D. O'Kelley, Phys. Rev. 129, 2591 (1963).

[13]H. K. Reynolds, D. N. F. Dunbar, W. A. Wenzel, and W. Whaling, Phys. Rev. 92, 742 (1953).

[14]J. B. Swint, R. M. Prior, and J. J. Ramirez, Nucl. Instr. Meth. 80, 134 (1970).

[15]C. C. Rousseau, W. K. Chu, and D. Powers, Phys. Rev. A (to be published).

[16]E. Bonderup, Kgl. Danske Videnskab. Selskab, Mat.-Fys. Medd. 35, No. 17 (1967).

[17]J. Lindhard and A. Winther, Kgl. Danske Videnskab. Selskab, Mat.-Fys. Medd. 34, No. 4 (1964).

[18]F. Herman and S. Skillman, *Atomic Structure Calculations* (Prentice-Hall, Englewood Cliffs, N. J., 1963).

PHYSICAL REVIEW B VOLUME 4, NUMBER 1 1 JULY 1971

Nuclear Spin-Lattice Relaxation and Dynamic Polarization in γ-Irradiated LiF †

K. M. Valentine and A. W. Nolle
Department of Physics, The University of Texas, Austin, Texas 78712
(Received 12 February 1971)

The spin-lattice relaxation at 13.6 MHz of F^{19} nuclei in γ-irradiated LiF is investigated at 300, 77, and 4.2–1.7 °K. The crystals used have optically determined *F*-center concentrations of 7.0×10^{17}, 2.0×10^{18}, and 3.5×10^{18} cm^{-3}. The relaxation in the temperature range 4.2–1.7 °K is found to be characterized by a spin-diffusion regime intermediate to the slow- and rapid-diffusion cases. At 300 °K, the nuclear spin-lattice relaxation is found to be predominantly controlled by *F*-center spin-lattice relaxation. However, for the *F*-center concentrations used here, temperature-independent *F*-center spin-spin relaxation is found to control the nuclear spin-lattice relaxation below 10 °K. The variation of the F^{19} dynamic polarization as a function of microwave power at 1.7 °K is investigated for microwave magnetic field amplitudes up to 2.6 G. For this range of fields, the dynamic polarization process also is characterized by an intermediate spin-diffusion regime. Existing theory yields an expression giving the variation of the dynamic polarization time with microwave power, which is used to estimate the correlation time of the *F*-center-nucleus dipole-dipole interaction at 1.7 °K. Estimates are also obtained for the *F*-center spin-lattice relaxation time at 300 °K.

INTRODUCTION

Bloembergen[1] has shown that nuclear magnetic spin-lattice relaxation in insulating crystalline solids at low temperatures can be caused by short-range direct magnetic dipolar interactions between the nuclei and paramagnetic impurity ions in low concentrations augmented by a nuclear spin-diffusion process. Nuclear spin diffusion has been exhaustively investigated[2–5] and the current state of the theory is such that it gives acceptable agreement with experiment. In addition to producing nuclear spin-lattice relaxation, the paramagnetic ion-nuclear dipolar interactions cause a mixing of the zero-order magnetic energy states which allows simultaneous nucleus-ion spin transitions, forbidden in zero order, to be induced by application of microwave radiation. Stimulation of the forbidden transitions results in a change in the nuclear magnetic polarization, which may be maintained at a steady-state value significantly different from the thermal equilibrium value. The process of produc-